

# Actin and myosin dynamics are independent during *Drosophila* embryonic wound repair

Anna B. Kobb<sup>a,b,†</sup>, Katheryn E. Rothenberg<sup>a,b,†</sup>, and Rodrigo Fernandez-Gonzalez<sup>a,b,c,d,\*</sup>

<sup>a</sup>Institute of Biomaterials and Biomedical Engineering, University of Toronto, Toronto, ON M5S 3G9, Canada;

<sup>b</sup>Ted Rogers Centre for Heart Research, University of Toronto, Toronto, ON M5G 1M1, Canada; <sup>c</sup>Department of Cell and Systems Biology, University of Toronto, Toronto, ON M5S 3G5, Canada; <sup>d</sup>Developmental and Stem Cell Biology Program, The Hospital for Sick Children, Toronto, ON M5G 1X8, Canada

**ABSTRACT** Collective cell movements play a central role in embryonic development, tissue repair, and metastatic disease. Cell movements are often coordinated by supracellular networks formed by the cytoskeletal protein actin and the molecular motor nonmuscle myosin II. During wound closure in the embryonic epidermis, the cells around the wound migrate collectively into the damaged region. In *Drosophila* embryos, mechanical tension stabilizes myosin at the wound edge, facilitating the assembly of a supracellular myosin cable around the wound that coordinates cell migration. Here, we show that actin is also stabilized at the wound edge. However, loss of tension or myosin activity does not affect the dynamics of actin at the wound margin. Conversely, pharmacological stabilization of actin does not affect myosin levels or dynamics around the wound. Together, our data suggest that actin and myosin are independently regulated during embryonic wound closure, thus conferring robustness to the embryonic wound healing response.

## Monitoring Editor

Richard Fehon  
University of Chicago

Received: Nov 8, 2018

Revised: Sep 17, 2019

Accepted: Sep 20, 2019

## INTRODUCTION

Coordinated cell behaviors mediate embryonic development in a wide variety of organisms, from worms and fruit flies to mice. Collective cell movements, for instance, drive cell sheet fusion during *Caenorhabditis elegans* ventral enclosure (Williams-Masson *et al.*, 1997), *Drosophila* dorsal closure (Kiehart *et al.*, 2000), and eyelid closure in the mouse (Heller *et al.*, 2014). Additionally, coordinated cellular movements have been implicated in cancer metastasis (Gaggioli *et al.*, 2007; Hidalgo-Carcedo *et al.*, 2011). Cell coordination generally requires redistribution of cytoskeletal proteins, resulting in the assembly of networks of actin and the motor protein

nonmuscle myosin II that span multiple cells and generate forces that pull cells together to produce cohesive behaviors.

Coordinated cell movements drive tissue repair in the embryonic epidermis. Embryonic wound healing is a conserved process in which the cells around the wound migrate into the wounded region, facilitating rapid and scarless repair. Upon wounding, the cells adjacent to the wound polarize actin and myosin to the wound edge, forming a supracellular, cable-like structure that encircles the wound (Martin and Lewis, 1992; Brock *et al.*, 1996; Kiehart *et al.*, 2000; Davidson *et al.*, 2002; Wood *et al.*, 2002). Cable contraction coordinates cell movements to close the wound (Wood *et al.*, 2002; Abreu-Blanco *et al.*, 2012; Fernandez-Gonzalez and Zallen, 2013).

We recently demonstrated that mechanical signals are critical for the dynamics of the cytoskeleton during embryonic wound closure. Strain or mechanical deformation drives myosin recruitment to the wound edge (Zulueta-Coarasa and Fernandez-Gonzalez, 2018), and tension stabilizes myosin at the wound margin (Kobb *et al.*, 2017). Loss of tension at the wound margin leads to faster myosin dynamics and an overall reduction in myosin levels at the wound edge. Conversely, the increase in tension around the wound associated with wound closure results in further stabilization of myosin. Computational modeling suggests that tension-based myosin stabilization at the wound edge is critical for efficient wound repair (Zulueta-Coarasa and Fernandez-Gonzalez, 2018). However, it is unclear

This article was published online ahead of print in MBoC in Press (<http://www.molbiolcell.org/cgi/doi/10.1091/mbc.E18-11-0703>) on September 25, 2019.

<sup>†</sup>These authors contributed equally to this work.

\*Address correspondence to: Rodrigo Fernandez-Gonzalez ([rodrigo.fernandez-gonzalez@utoronto.ca](mailto:rodrigo.fernandez-gonzalez@utoronto.ca)).

Abbreviations used: ABD, actin-binding domain; DMSO, dimethyl sulfoxide; dsRNA, double-stranded RNA; FRAP, fluorescence recovery after photobleaching; GFP, green fluorescent protein; Jasp, jasplakinolide; LatA, latrunculin A;  $t_{1/2}$ , half time of fluorescence recovery after photobleaching; zip, zipper.

© 2019 Kobb, Rothenberg, and Fernandez-Gonzalez. This article is distributed by The American Society for Cell Biology under license from the author(s). Two months after publication it is available to the public under an Attribution-Noncommercial-Share Alike 3.0 Unported Creative Commons License (<http://creativecommons.org/licenses/by-nc-sa/3.0>).

"ASCB®," "The American Society for Cell Biology®," and "Molecular Biology of the Cell®" are registered trademarks of The American Society for Cell Biology.

whether tension affects myosin motors directly, or whether the stabilization of myosin by tension occurs indirectly through actin, which largely colocalizes with myosin at the wound edge (Zulueta-Coarasa and Fernandez-Gonzalez, 2018).

Mechanical signals can control actin dynamics through several tension-sensitive actin regulators. The formin Diaphanous promotes processive actin elongation (Romero *et al.*, 2004) and is important for actin cable formation during wound repair (Matsubayashi *et al.*, 2015). Diaphanous can promote faster actin polymerization in filaments that sustain tension (Courtemanche *et al.*, 2013; Higashida *et al.*, 2013; Jegou *et al.*, 2013). Binding of the actin-severing protein cofilin to actin is slower when actin filaments are under increased tension (Hayakawa *et al.*, 2011), and thus tension may also prevent actin filament disassembly, which may indirectly affect myosin dynamics. However, recent data suggest that the dynamics of myosin and actin are independent (Hu *et al.*, 2017). Consistent with this, myosin still polarizes at the wound margin in *diaphanous* mutants, albeit more slowly than in controls and in a patchy pattern (Matsubayashi *et al.*, 2015). Thus, it is currently unclear whether actin and myosin are jointly regulated during embryonic wound repair.

## RESULTS

### Actin is stabilized around embryonic wounds

We used fluorescence recovery after photobleaching (FRAP) to investigate whether actin is regulated by tension during embryonic wound closure. We wounded the epidermis of *Drosophila* embryos expressing green fluorescent protein (GFP):Utrophin actin-binding domain (ABD), a reporter for filamentous actin (Rauzi *et al.*, 2010), at stages 14–15 of embryonic development (~12 h postfertilization). We conducted our measurements within the fast phase of wound closure, when wound area was ~50% of its maximum (Abreu-Blanco *et al.*, 2012; Fernandez-Gonzalez and Zallen, 2013; Kobb *et al.*, 2017). At this stage, cable contraction is the dominant mechanism coordinating cell movement (Wood *et al.*, 2002; Zulueta-Coarasa and Fernandez-Gonzalez, 2018). We compared actin dynamics in the supracellular cables at the wound margin and in the cables that segment the epidermis at the same developmental stage (Simone and DiNardo, 2010) (Figure 1, A and B). We previously showed that wound edge cables sustain greater tension than epidermal cables (Kobb *et al.*, 2017). Similar to myosin, actin fluorescence was also greater at the wound edge than in epidermal cables (Figure 1C). We found that actin dynamics at the wound edge had a characteristic time,  $t_{1/2}$  (the time necessary for half of the maximum fluorescence recovery in FRAP experiments), of  $28 \pm 4$  s (mean  $\pm$  SEM; Figure 1, D and E). In epidermal cables, GFP:UtrophinABD displayed a  $t_{1/2}$  of  $7 \pm 1$  s, significantly shorter than at the wound margin ( $p < 0.002$ ; Figure 1, D and E), with no differences in the mobile fraction (the amount of fluorescence recovery; Figure 1, D and F). We obtained similar results using an additional marker for filamentous actin, the actin cross-linking protein Filamin, tagged with GFP (Huelsmann *et al.*, 2016) (Supplemental Figure S1, A–F). Specifically, the  $t_{1/2}$  of Filamin:GFP at the wound margin was  $27 \pm 3$  s, similar to that of GFP:UtrophinABD. Filamin:GFP dynamics were also slower at the wound edge with respect to epidermal cables, where the  $t_{1/2}$  of Filamin:GFP was significantly shorter ( $10 \pm 2$  s,  $p < 0.01$ ; Supplemental Figure S1, D and E).

To investigate whether tension affected actin polymerization or depolymerization at the cortex, we used mathematical modeling of our FRAP data to extract the rates of actin assembly ( $k_{on}$ ) and disassembly ( $k_{off}$ ) in the photobleached regions (Kobb *et al.*, 2017) (see *Materials and Methods*). Using GFP:UtrophinABD, our analysis indicated that actin assembly at the wound edge occurred at a rate 87%

slower than in epidermal cables ( $0.011 \pm 0.004$  s<sup>-1</sup> vs.  $0.085 \pm 0.020$  s<sup>-1</sup>, respectively,  $p < 0.01$ ; Figure 1G). The rate of actin disassembly at the wound edge was 78% slower than in epidermal cables ( $0.020 \pm 0.0035$  s<sup>-1</sup> vs.  $0.091 \pm 0.0098$  s<sup>-1</sup>,  $p < 0.01$ ; Figure 1H). Similar results were obtained using Filamin:GFP (Supplemental Figure S1, G and H). Together, these data suggest that both actin assembly and disassembly occur at significantly lower rates at the wound edge than in other supracellular actin networks that sustain reduced tension.

The results of FRAP experiments using GFP:UtrophinABD and Filamin:GFP could reflect the rate of assembly of a subset of actin filaments that can be bound by these markers of F-actin. To validate that the dynamics of F-actin reporters corresponded to the dynamics of actin, we conducted FRAP experiments in embryos expressing GFP:Act5C, a fluorescently tagged monomeric actin that can be incorporated into filamentous structures (Roper *et al.*, 2005) (Supplemental Figure S2, A–H). Similar to GFP:UtrophinABD and Filamin:GFP, GFP:Act5C displayed a significantly longer  $t_{1/2}$  at the wound margin compared with epidermal cables ( $16.9 \pm 3.4$  s vs.  $3.4 \pm 0.4$  s, respectively,  $p < 0.002$ ; Supplemental Figure S2, D and E), and no differences were found in the mobile fractions (Supplemental Figure S2F). Furthermore, mathematical modeling suggested that the slower dynamics of GFP:Act5C at the wound edge were due to reduced rates of both actin assembly and disassembly (Supplemental Figure S2, G and H). Together, our data strongly indicate that actin is stabilized at the wound edge during embryonic tissue repair.

### Actin dynamics at the wound edge are largely independent of tension

Our data suggest that tension may stabilize actin at the wound margin. To determine whether tension regulates actin localization around embryonic wounds, we quantified actin fluorescence after reducing tension at the wound edge. We used laser ablation to sever the actomyosin cable, partially releasing the tension that it sustained. We conducted the release of tension 10 min after wounding embryos expressing GFP:Utrophin:ABD. We monitored fluorescence at the wound edge in regions adjacent to the site of ablation (Figure 2A), far (at least 10  $\mu$ m away; Figure 2A'), and in sham-irradiated controls (Figure 2A''). Within 100 s of severing the cable, we measured a significant loss of  $15 \pm 6\%$  of GFP:UtrophinABD fluorescence in regions of the wound edge adjacent to the point of ablation ( $p < 0.05$ , 16 of 22 regions displayed a decrease in fluorescence; Figure 2, B and C). In contrast, there was no loss of fluorescence in segments of the wound edge far from the ablation site or in sham-irradiated controls (Figure 2, B'–B'' and C–C'). We obtained similar results when we monitored actin levels at the wound edge in embryos expressing GFP:Act5C (Supplemental Figure S3, A and B). GFP:Act5C fluorescence at the wound edge in regions adjacent to the site of ablation decreased by  $34 \pm 7\%$  100 s after releasing tension ( $p < 0.001$ , 13 of 14 regions displayed a decrease in fluorescence; Supplemental Figure S3, C and C'). Thus, similar to our previous findings with myosin (Kobb *et al.*, 2017), our data indicate that tension is in part necessary to maintain actin at the wound margin.

The formin Diaphanous localizes to the wound margin, where it is necessary for the assembly of the actin cable (Matsubayashi *et al.*, 2015). Diaphanous activity and localization can be regulated by tension (Courtemanche *et al.*, 2013; Higashida *et al.*, 2013; Jegou *et al.*, 2013). Thus, we predicted that Diaphanous may display sensitivity to tension in its localization to the wound edge. To test this possibility, we quantified changes in the localization of

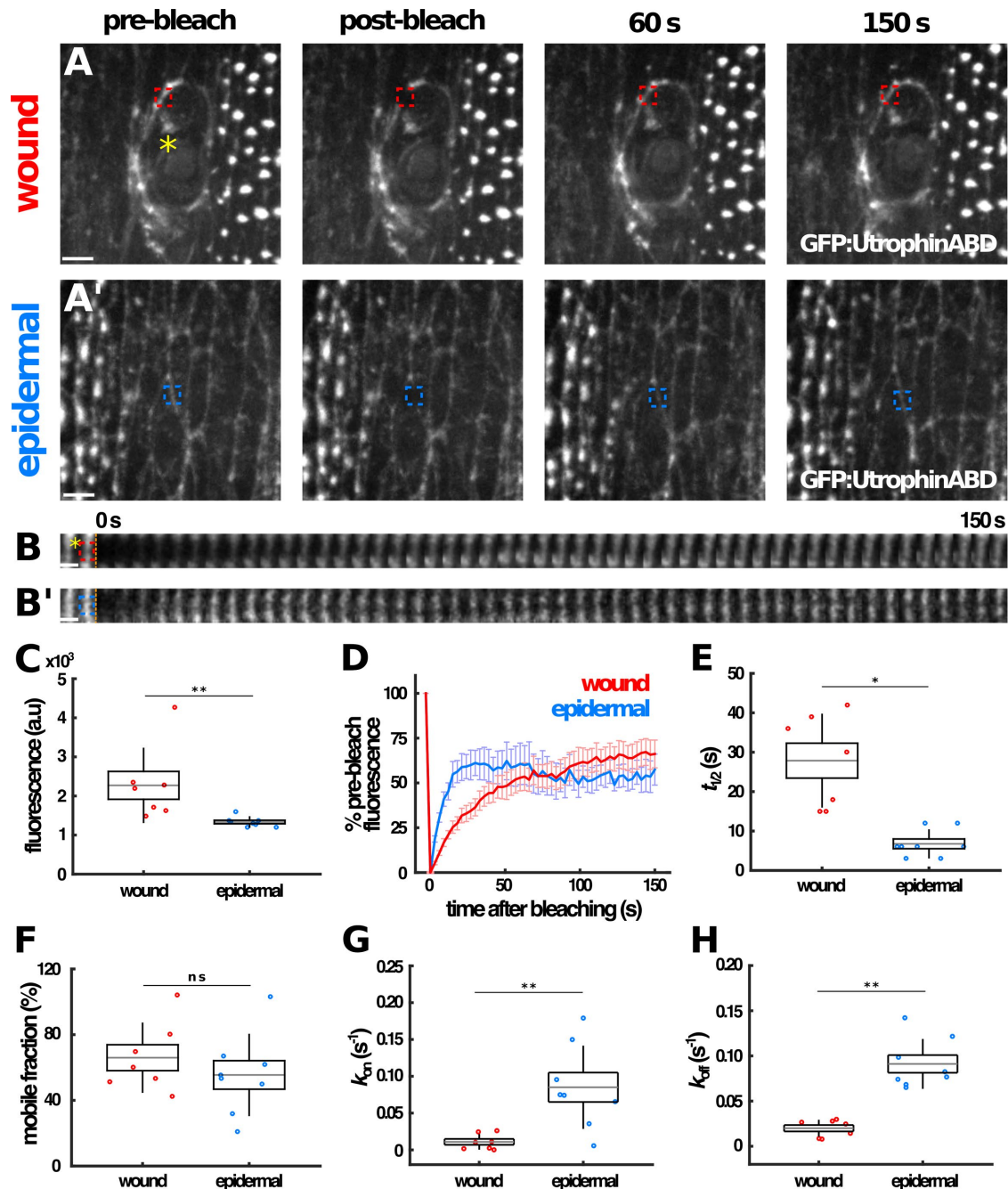


**FIGURE 1:** GFP:UtrophinABD is stabilized at the wound margin. (A) FRAP experiments in cables at the wound edge (A, red) and in epidermal cables (A', blue) in embryos expressing GFP:UtrophinABD. Scale bars, 5  $\mu$ m. (B) Kymographs corresponding to the experiments shown in A. Orange dashed lines indicate the time of photobleaching. Scale bars, 3 s. (A, B) Yellow asterisks indicate the position of the wound. Anterior left, ventral down. (C–H) Initial fluorescence (C), the percentage of prebleach fluorescence over time in the photobleached region (D),  $t_{1/2}$  (E), mobile fraction (F), assembly rate (G), and disassembly rate (H) for FRAP experiments in cables around wounds (red,  $n = 7$  photobleached regions in as many embryos), and epidermal cables (blue,  $n = 8$ ); a.u., arbitrary units. (C, E–H) For box plots, error bars show the SD, the box indicates the standard error of the mean (SEM), and gray lines denote the mean. ns: not significant, \* $p < 0.05$ , \*\* $p < 0.01$  (Mann–Whitney test). (D) Error bars, SEM.

GFP:Diaphanous when the actin cable was severed (Figure 3, A and B). We found that in segments of the wound edge adjacent to the site of tension release, GFP:Diaphanous fluorescence decreased by  $15 \pm 6\%$  within 100 s ( $p < 0.05$ , 11/14 segments displayed a reduction in fluorescence; Figure 3, B and C). GFP:Diaphanous fluorescence remained relatively constant over the same period of time in

segments of the wound edge far from the ablation site or in sham-irradiated controls (Figure 3, B'–B'', C, and C'). Together, these data strongly indicate that Diaphanous is partly regulated by tension during embryonic wound closure.

To investigate whether tension regulates the dynamics of the pool of actin that remains at the wound edge after tension release, we

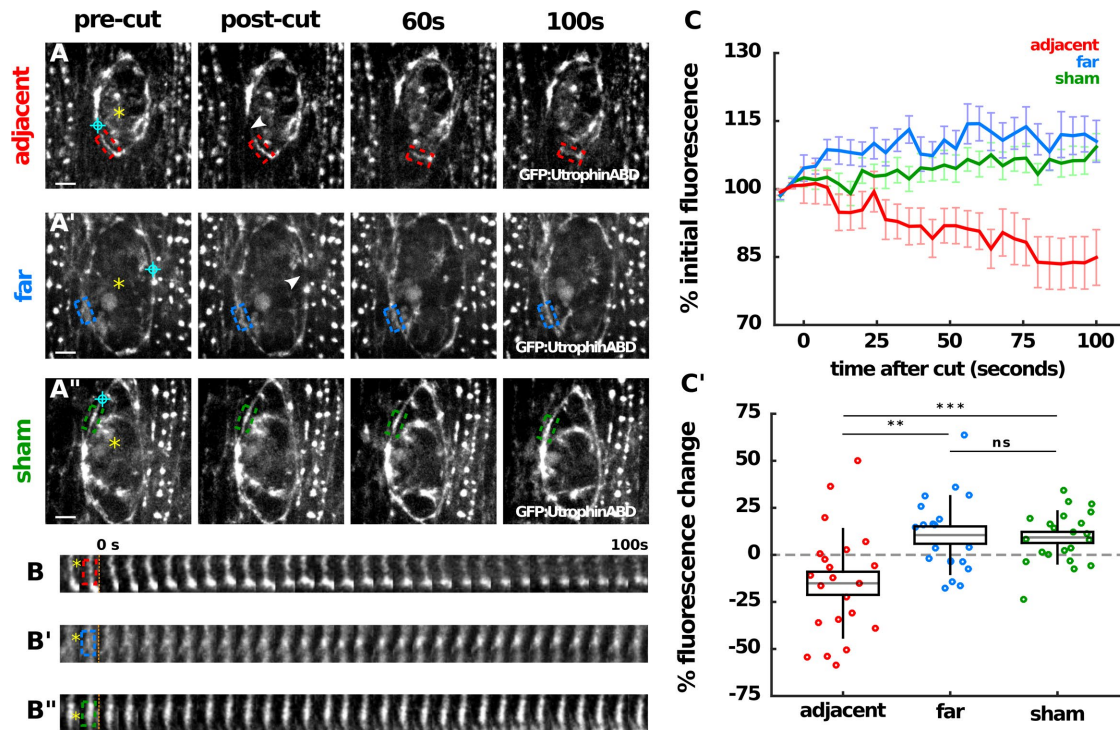


**FIGURE 2:** Tension is partially necessary for actin localization at the wound margin. (A, B) Still images (A–A'') and kymographs (B–B'') showing GFP:UtrophinABD levels in regions of the wound edge adjacent to the site of tension release (red, A, B), far away (blue, A', B'), and in sham-irradiated controls (green, A'' and B''). Cyan targets and white arrowheads indicate ablation sites. Yellow asterisks show the position of the wound. Boxes display the region where fluorescence was monitored. Anterior left, ventral down. Scale bars, 5  $\mu\text{m}$  (A–A'') or 4 s (B–B''). (B) Orange dashed lines indicate the time of irradiation. (C–C') GFP:UtrophinABD fluorescence normalized to the fluorescence before severing the wound edge (C), and the percentage of change in GFP:UtrophinABD fluorescence 100 s after severing the wound edge (C') for regions adjacent to the site of ablation (red,  $n = 22$  regions), far (blue,  $n = 21$ ), or in sham-irradiated controls (green,  $n = 22$ ). (C) Error bars indicate SEM. (C') Error bars show the SD, the box indicates SEM, and gray lines denote the mean; ns: not significant,  $**p < 0.005$ ,  $***p < 0.001$  (Kruskal–Wallis and Dunn's test).

conducted FRAP experiments at the wound margin  $\sim 1$  min after reducing tension in embryos expressing GFP:UtrophinABD (Figure 4, A and B). Actin dynamics did not change significantly in regions adjacent to the site of ablation compared with regions at least 10  $\mu\text{m}$  away or in sham-irradiated controls ( $t_{1/2}$  of  $24 \pm 3$  s,  $27 \pm 3$  s, and  $29 \pm 3$  s, respectively; Figure 4, C–E). Furthermore, mathematical modeling suggested that neither the rate of actin assembly nor the rate of actin disassembly was affected by the loss of tension (Figure 4, F and G). Together, these results suggest that the dynamics of the majority of actin at the wound edge are independent of mechanical forces.

To further probe the effects of tension on actin during wound closure, we investigated whether tension is sufficient to stabilize actin around wounds by comparing GFP:UtrophinABD dynamics during early (50% maximum wound area), mid (30% maximum wound area), and late ( $< 10\%$  maximum wound area) stages of wound repair (Figure 5, A and B). Tension around the wound margin increases as wound closure progresses (Kobb *et al.*, 2017), and thus we hypothesized that if tension stabilized actin at the wound edge, the  $t_{1/2}$  for GFP:UtrophinABD would increase as wounds closed. However, we found no significant changes in the  $t_{1/2}$  of GFP:UtrophinABD at the wound margin as wounds closed ( $26 \pm 2$  s,  $21 \pm 3$  s, and  $27 \pm 4$  s in early, mid, and late wound repair, respectively; Figure 5, C–E). Similar results were obtained using Filamin:GFP to monitor actin dynamics (Supplemental Figure S4, A–E). Taken together, our data indicate that, unlike with myosin (Kobb *et al.*, 2017), tension does not control the dynamics of a large pool of actin at the wound edge, suggesting

that actin and myosin may be independently regulated during embryonic wound closure.

### Actin dynamics at the wound edge are independent of myosin

Our results suggest that actin and myosin may be regulated independently around embryonic wounds. To investigate the interplay between myosin and actin dynamics during wound closure, we quantified the dynamics of actin when myosin levels were reduced. We injected embryos expressing E-cadherin:tdTomato and a GFP-tagged form of the myosin regulatory light chain (MRLC) (Royou *et al.*, 2004) (myosin:GFP) with double-stranded RNA (dsRNA) against *zipper* (*zip*), the *Drosophila* gene that encodes the nonmuscle myosin II heavy chain. The *zip* dsRNA treatment resulted in a 38% decrease in the amount of myosin at epidermal cables with respect to water-injected controls (Supplemental Figure S5, A and B). The reduction in myosin levels in *zip* dsRNA embryos was associated with an overexpansion of the wound, a significant delay in wound closure, and reduced myosin levels at the wound edge (Supplemental Figure S5, C–E), consistent with our previous findings in embryos expressing mutant forms of myosin with reduced motor activity (Kobb *et al.*, 2017).

Next, we conducted FRAP experiments in embryos expressing GFP:UtrophinABD that had been treated with *zip* dsRNA (Figure 6, A and B). To maintain consistent wound sizes between groups during FRAP experiments, wounds in dsRNA-treated embryos were allowed

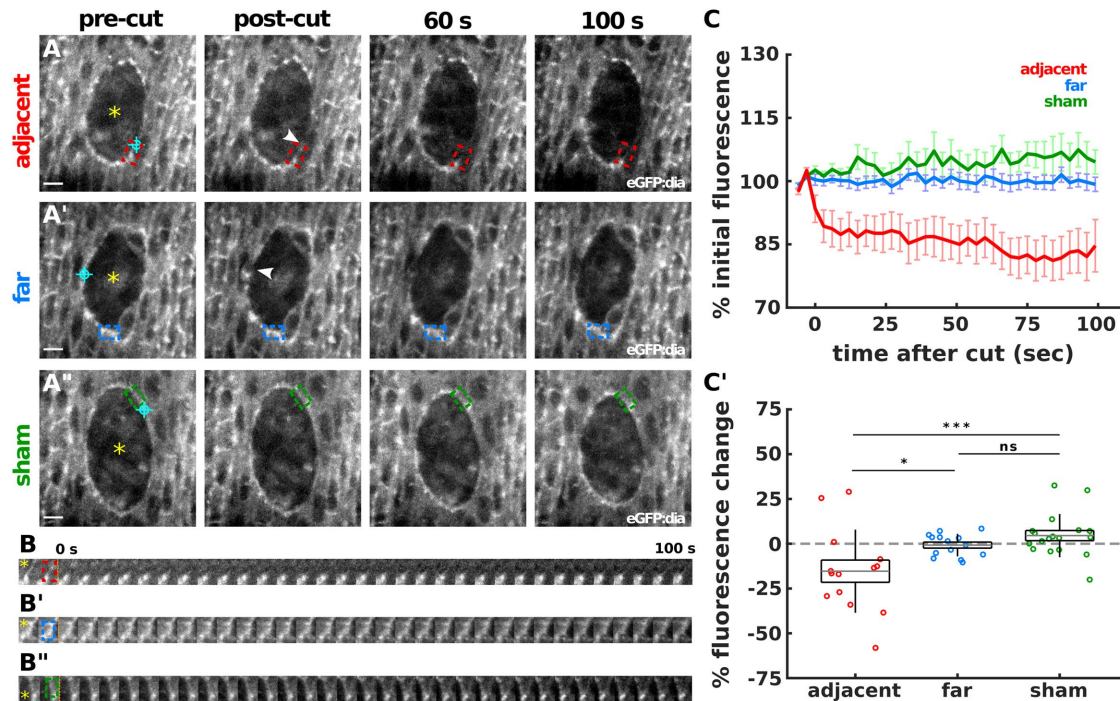


**FIGURE 3:** Tension is partially necessary for Diaphanous localization at the wound margin. (A, B) Still images (A–A'') and kymographs (B–B'') showing GFP:Diaphanous levels in regions of the wound edge adjacent to the site of tension release (red, A, B), far away (blue, A', B'), and in sham-irradiated controls (green, A'', B''). Cyan targets and white arrowheads indicate ablation sites. Yellow asterisks show the position of the wound. Boxes display the region where fluorescence was monitored. Anterior left, ventral down. Scale bars, 5  $\mu$ m (A–A'') or 3 s (B–B''). (B) Orange dashed lines indicate the time of irradiation. (C–C') GFP:Diaphanous fluorescence normalized to the fluorescence before severing the wound edge (C), and the percentage of change in GFP:Diaphanous fluorescence 100 s after severing the wound edge (C'), for regions adjacent to the site of ablation (red,  $n = 14$  regions), far (blue,  $n = 14$ ), or in sham-irradiated controls (green,  $n = 18$ ). (C) Error bars indicate SEM. (C') Error bars show the SD, the box indicates SEM, and gray lines denote the mean; ns: not significant, \* $p < 0.05$ , \*\*\* $p < 0.001$  (Kruskal–Wallis and Dunn's test).

to close until wound size was comparable to the water-injected group at 50% closure. In spite of the defects in wound closure and reduced myosin levels at the wound margin, the dynamics of the pool of actin at the wound edge were not affected by the loss of myosin: the  $t_{1/2}$  of fluorescence recovery was  $24 \pm 3$  s, similar to the  $22 \pm 2$  s in water-injected controls, and with comparable mobile fractions (Figure 6, C–E). We validated these results by examining the dynamics of actin during wound closure in embryos in which myosin activity was acutely inhibited by treatment with 10 mM of Y-27632, an inhibitor of Rho-kinase that blocks myosin activity in the embryo (Bertet et al., 2004; Fernandez-Gonzalez et al., 2009; Kobb et al., 2017) and disrupts wound closure (Supplemental Figure S6, A and B) (Fernandez-Gonzalez and Zallen, 2013; Verboon and Parkhurst, 2015; Kobb et al., 2017). Acute myosin inhibition when wounds had closed to ~50% of their maximum area in embryos expressing GFP:UtrrophinABD did not affect the dynamics of actin at the wound edge: the  $t_{1/2}$  of fluorescence recovery was  $22 \pm 4$  s, similar to the  $28 \pm 4$  s in water-injected controls (Supplemental Figure S7, A–E). Together, our data indicate that actin dynamics in the contractile cable around embryonic wounds are largely independent of myosin.

### Myosin stabilization at the wound edge is independent of actin

Our data suggest that a significant population of actin at the wound margin is regulated independently of myosin. Notably, in rat embryonic fibroblasts the dynamics of myosin in filaments are indepen-

dent of actin, but become actin-dependent when myosin filaments align into higher order structures (Hu et al., 2017). To establish whether myosin dynamics at the wound edge depend on actin dynamics, we stabilized actin by coinjecting embryos with 1 mM of jasplakinolide and 1 mM of latrunculin A. Jasplakinolide inhibits actin depolymerization by tightly binding and stabilizing filaments (Bubb et al., 1994, 2000; Cramer, 1999; Wilson et al., 2010). Latrunculin A sequesters actin monomers, effectively inhibiting polymerization (Spector et al., 1983; Coue et al., 1987). Thus, the combination of jasplakinolide and latrunculin A treatments stabilizes actin filaments in cultured cells (Hansen and Mullins, 2015; Hu et al., 2017). We found that coinjection of 1 mM jasplakinolide and 1 mM latrunculin A (hereafter referred to as Jasp/LatA) into embryos expressing GFP:Act5C significantly reduced actin dynamics during embryonic wound closure (Supplemental Figure S8, A–C). In FRAP experiments, the mobile fraction of GFP:Act5C at the wound edge decreased from  $70 \pm 6\%$  in control embryos injected with dimethyl sulfoxide (DMSO) to  $26 \pm 6\%$  in Jasp/LatA-treated embryos ( $p < 0.005$ ; Supplemental Figure S8, C–E). Thus, Jasp/LatA treatment stabilizes actin in *Drosophila* embryos.

Next, we investigated whether actin stabilization disrupted myosin dynamics around embryonic wounds. We injected embryos expressing myosin:GFP with Jasp/LatA when wounds reached ~50% of their maximum area. Two minutes after injection, we photo-bleached the myosin cable at the wound margin (Figure 7, A and B). Stabilizing actin with Jasp/LatA did not cause a significant effect in

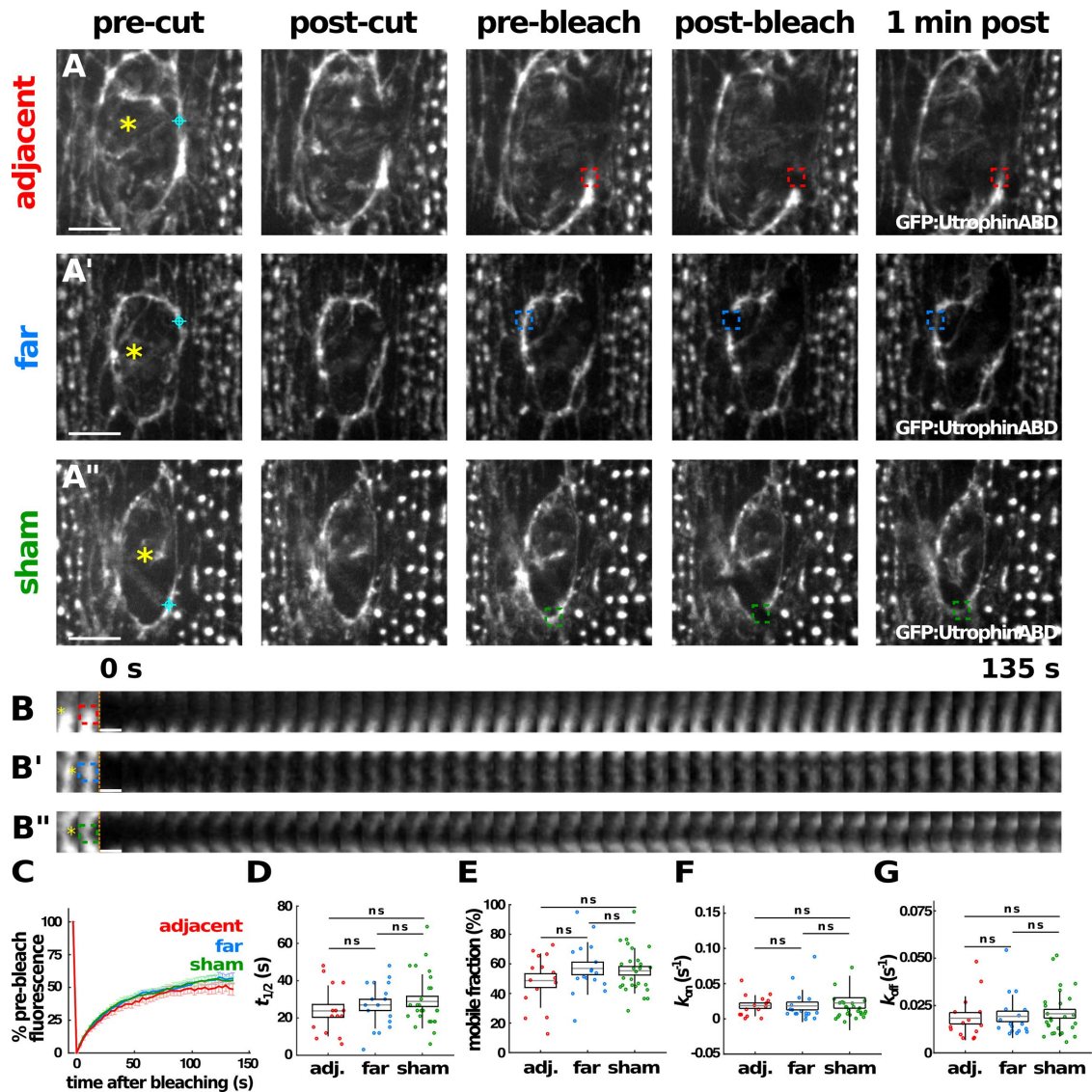


**FIGURE 4:** Reducing tension does not change actin dynamics at the wound edge. (A, B) Still images (A–A'') and kymographs (B–B'') showing FRAP experiments in wounded embryos expressing GFP:UtrophinABD and irradiated with an ultraviolet laser to reduce tension (A–A', B–B'), or sham-irradiated (A'', B''). Images show a region adjacent to the ablation site (red, A, B), far (blue, A', B'), or in a sham-irradiated control (green, A'', B''). Cyan targets indicate ablation sites. Orange dashed lines indicate the time of photobleaching. Anterior left, ventral down. Scale bars, 10  $\mu$ m (A–A'') and 4 s (B–B''). (C–G) The percentage of prebleach GFP:UtrophinABD fluorescence over time in the photobleached region (C),  $t_{1/2}$  (D), mobile fraction (E), assembly rate (F), and disassembly rate (G) for regions adjacent (red,  $n = 15$  regions) or far (blue,  $n = 17$ ) from the ablation site, and in sham-irradiated controls (green,  $n = 27$ ). (C) Error bars indicate SEM. (D–G) Error bars show the SD, the box indicates SEM, and gray lines denote the mean; ns: not significant (Kruskal–Wallis test).

the myosin levels at the wound margin (Figure 7, A, insets, and C), but affected the rate of wound closure (Supplemental Figure S9, A and B). Importantly, the rate of FRAP was the same for Jasp/LatA-injected and DMSO-treated controls (Figure 7, D–F). Similar results were obtained when we treated embryos with cytochalasin D. Cytochalasin D stabilizes actin by binding to the growing end of the filament and preventing monomer addition (Flanagan and Lin, 1980). We found that treatment with 1 mM of cytochalasin D resulted in a significant reduction in the mobile fraction of GFP:Act5C in FRAP experiments ( $p < 0.02$ ; Supplemental Figure S10, A–E). Similar to Jasp/LatA treatment, cytochalasin D did not affect myosin levels (Supplemental Figure S11, A, insets, and C) or the dynamics of myosin during wound closure (Supplemental Figure S11, A–F).

Together, our data indicate that both myosin and actin dynamics are largely independent around embryonic wounds.

## DISCUSSION

Our results show that, similar to our previous findings with myosin (Kobb *et al.*, 2017), actin dynamics are slowed down at the wound margin during embryonic wound repair. However, in contrast with myosin, increasing or decreasing tension around the wound does not change actin dynamics. Myosin generates tension as wounds close (Fernandez-Gonzalez and Zallen, 2013), and thus our data suggest that actin and myosin may be independently regulated at the wound edge. We validated our hypothesis experimentally by showing that actin stabilization during wound closure does not

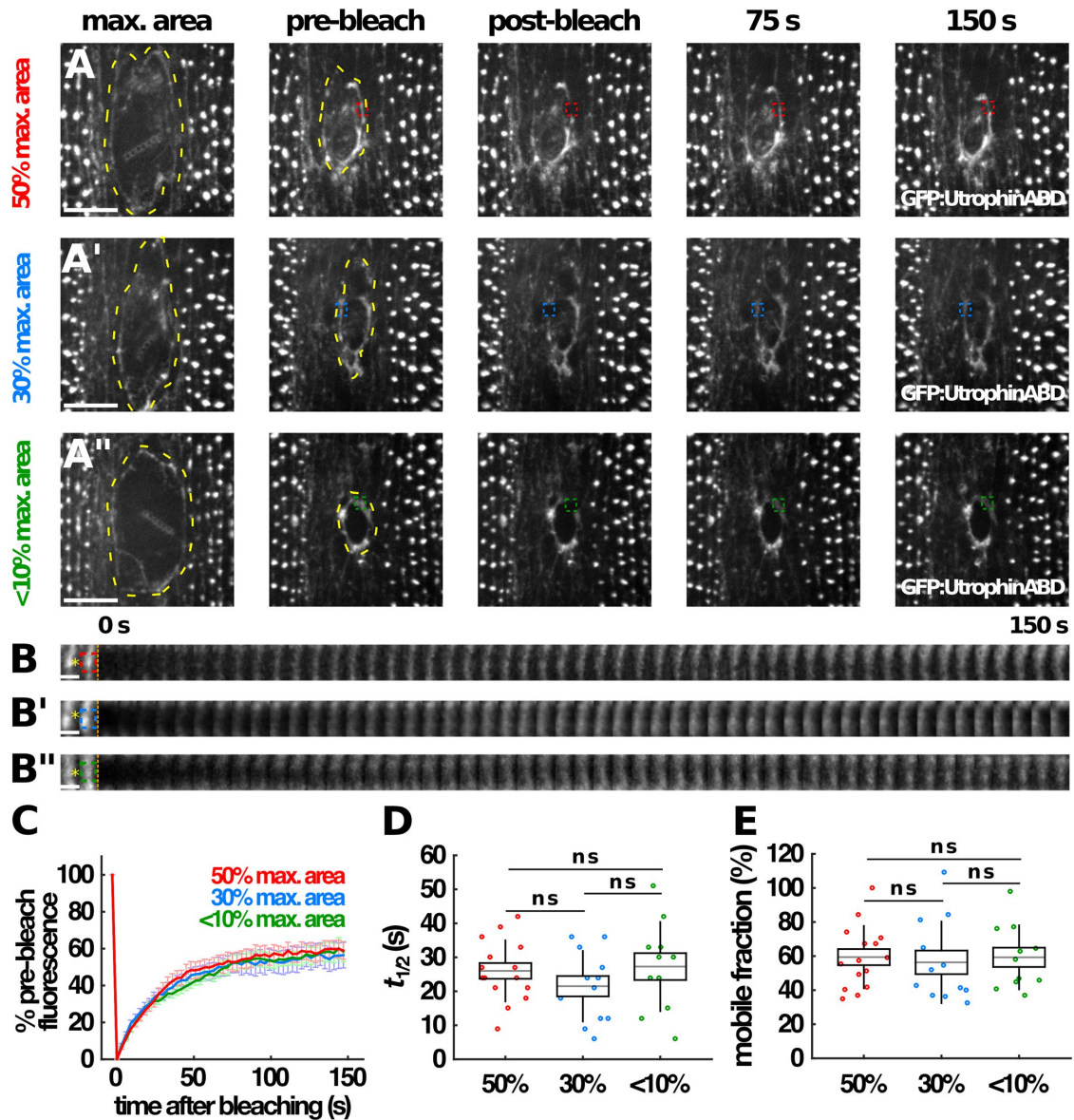


**FIGURE 5:** Increasing tension does not change actin dynamics at the wound edge. (A, B) Stills (A–A'') and corresponding kymographs (A'–B') of FRAP experiments at the wound edge during the early stages of wound repair (~50% of the maximum wound area, A, B, red), intermediate (~30% of the maximum wound area, A', B', blue), or late in the repair process (less than 10% of the maximum wound area, A'', B'', green), in embryos expressing GFP:UtrophinABD. Yellow dashed lines outline the wounds at their maximum area and at the time point prior to photobleaching. Orange dashed lines show the time of photobleaching. Anterior left, ventral down. Scale bars, 10  $\mu$ m (A–A'') and 3 s (B–B''). (C–E) The percentage of prebleach fluorescence over time in the photobleached region (C),  $t_{1/2}$  (D), and mobile fraction (E), for FRAP experiments during early (red,  $n = 15$  regions), mid (blue,  $n = 12$ ), and late wound closure (green,  $n = 11$ ). (C) Error bars indicate SEM. (D, E) Error bars show the SD, the box indicates the SEM, and gray lines denote the mean; ns: not significant (Kruskal–Wallis test).

affect myosin dynamics, and conversely, the dynamics of actin at the wound edge are largely independent of myosin levels or activity. Of note, we showed that a small pool of actin was rapidly lost from the wound edge when tension or myosin were disrupted. Thus, we report, for the first time to our knowledge, the presence of two pools of actin around embryonic wounds, a larger, tension-independent pool, and smaller, tension-dependent one.

In mammalian cells in culture, the dynamics of myosin filaments in stress fibers and cortical arcs are independent of actin (Hu *et al.*, 2017). In contrast, in the lamellipodia and lamellae of fish and amphibian cells, actin dynamics are directly affected by myosin activity

(Yamashiro *et al.*, 2018). We previously found that actin and myosin colocalize at the edge of wounds in *Drosophila* embryos (Zulueta-Coarasa and Fernandez-Gonzalez, 2018). Strikingly, here we show that actin and myosin dynamics at the supracellular cable around embryonic wounds are largely independent of each other despite their strong colocalization.

An actomyosin cable drives embryonic wound healing. Actin and myosin generate contractile forces to coordinate cell movements and close the wound (Martin and Lewis, 1992; Brock *et al.*, 1996; Kiehart *et al.*, 2000; Wood *et al.*, 2002; Zulueta-Coarasa and Fernandez-Gonzalez, 2018). The formin Diaphanous is necessary for actin

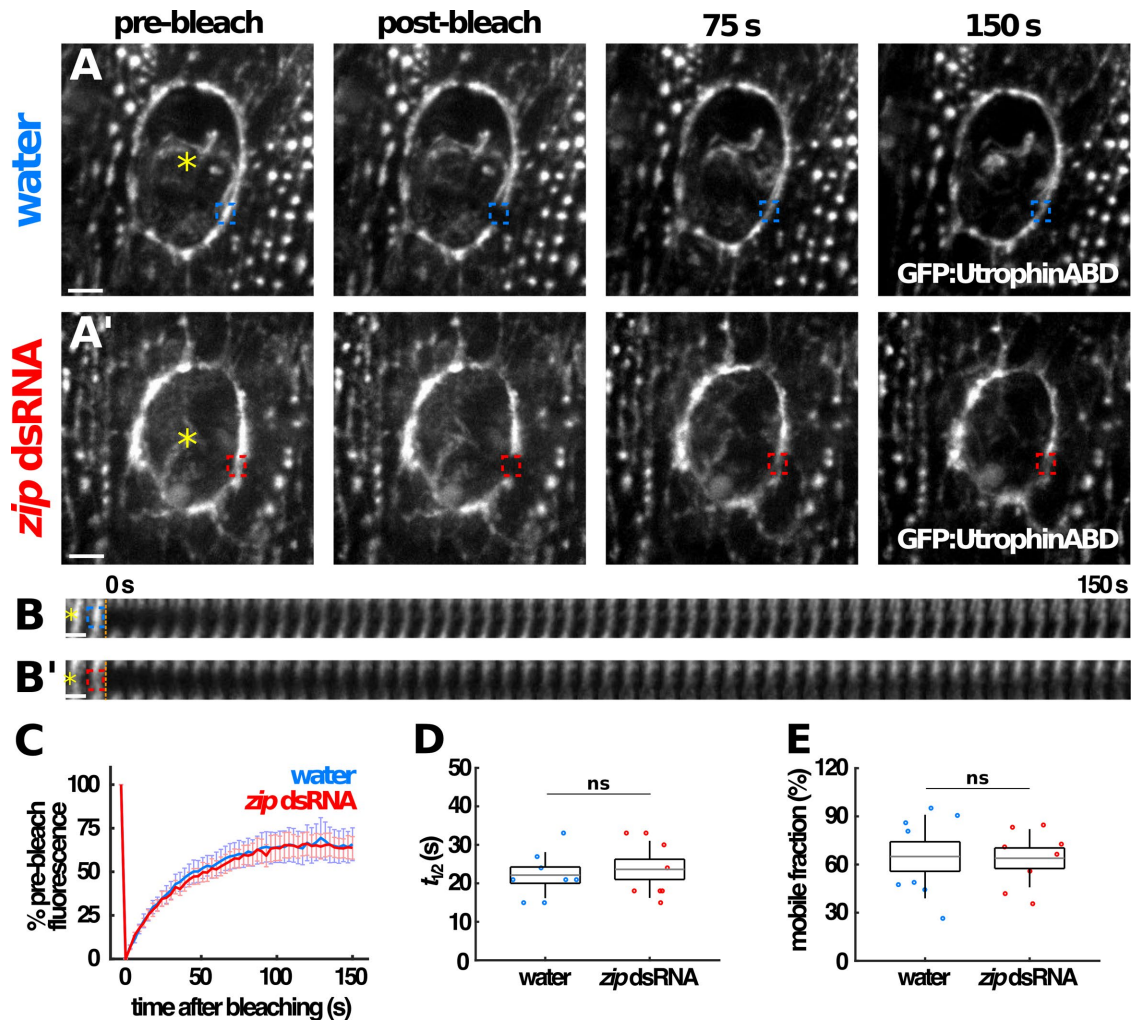


**FIGURE 6:** Actin dynamics do not change when myosin levels are reduced. (A, B) FRAP experiments in wounded embryos expressing GFP:UtrophinABD and injected with water (A, blue) or *zip* dsRNA (A', red) and corresponding kymographs (B–B'). Yellow asterisks indicate the position of the wound. Orange dashed lines indicate the time of photobleaching. Anterior left, ventral down. Scale bars, 10  $\mu$ m (A–A'), 3 s (B–B'). (C–E) The percentage of prebleach fluorescence over time in the photobleached region (C),  $t_{1/2}$  (D) and mobile fraction (E) for wounds in embryos injected with water (blue,  $n = 8$  regions) or with *zip* dsRNA (red,  $n = 8$ ). (C) Error bars indicate SEM. (D, E) Error bars show SD, the box indicates SEM, and gray lines denote the mean; ns: not significant (Mann–Whitney test).

cable assembly (Matsubayashi *et al.*, 2015). Formin activity can be regulated by mechanical signals (Courtemanche *et al.*, 2013; Higashida *et al.*, 2013; Jegou *et al.*, 2013), and our data show that the localization of Diaphanous to the wound margin depends in part on tension. Thus, myosin-induced tension may promote formin activity and actin polymerization at the wound edge.

Other molecular mechanisms may contribute to embryonic wound repair. In yeast, actin filament severing can induce contraction of cytokinetic rings, even in the absence of myosin activity (Mendes Pinto *et al.*, 2012). During *Drosophila* pupal development, wound closure and actin polarization to the wound edge depend on the actin filament-severing protein gelsolin (Antunes *et al.*, 2013). Contraction based on actin filament disassembly requires the presence of actin cross-linkers that can reestablish the connection between filaments after they have been severed (Zumdieck *et al.*, 2007). Therefore, a tension-insensitive actin pool at the wound edge may promote motorless contraction when combined with actin cross-linkers, thus providing an additional

layer of redundancy in embryonic wound healing. Experiments investigating the effect of myosin inhibition on actin dynamics when individual actin regulators and cross-linkers have been silenced will reveal which actin pools are (in)sensitive to myosin motor activity. Together, our results reveal an intricate relationship between cytoskeletal networks and regulators thereof, that must be exquisitely coordinated during the cell movements that drive tissue repair.

## MATERIALS AND METHODS

### Fly stocks

Live imaging was conducted using *endo-DE-cadherin:tdTomato* (Huang *et al.*, 2009), *sqh-sqh:GFP* (*sqh* encodes the MRLC) (Royou *et al.*, 2004), *sqh-GFP:UtrophinABD* (Rauzi *et al.*, 2010), *cher:GFP* (*cher* encodes Filamin) (Huelsmann *et al.*, 2016), *UAS-GFP:Act5C* (Roper *et al.*, 2005), and *UAS-GFP:dia* (Homem and Peifer, 2008). UAS constructs were ubiquitously driven with *tubulin-Gal4* (Lee and Luo, 1999).

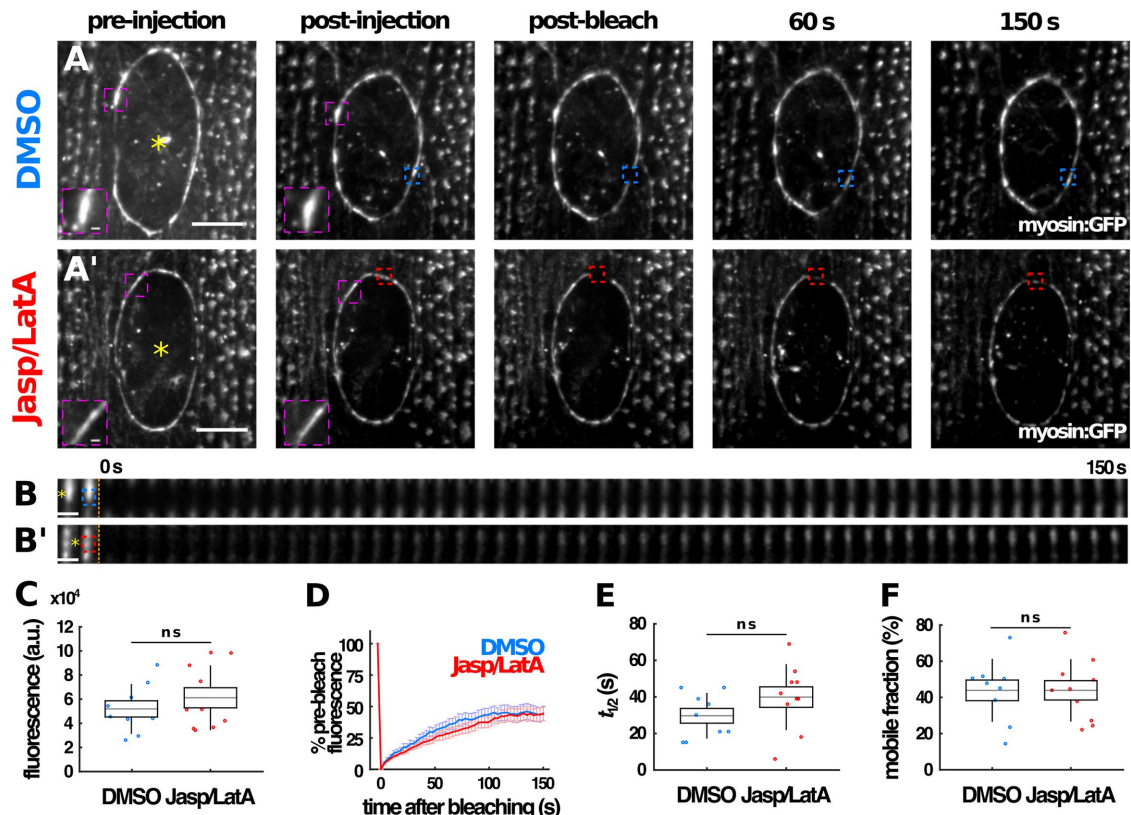


**FIGURE 7:** Actin stabilization does not affect myosin dynamics during wound repair. (A, B) FRAP experiments in wounded embryos expressing myosin:GFP and injected with DMSO (A, blue) or with Jasp/LatA cocktail (A', red) and corresponding kymographs (B–B'). Yellow asterisks indicate the position of the wound. Insets show a zoom into a region of the wound margin. Orange dashed lines indicate the time of photobleaching. Anterior left, ventral down. Scale bars, 10  $\mu\text{m}$  (A–A') or 3 s (B–B'). (C–F) Myosin fluorescence 2 min after injection just prior to photobleaching (C), the percentage of prebleach fluorescence over time in the photobleached region (D),  $t_{1/2}$  (E), and mobile fraction (F) for wounds in embryos injected with DMSO (blue,  $n = 9$  regions) or Jasp/LatA (red,  $n = 10$ ). (C, E, F) Error bars show SD, the box indicates SEM, and gray lines denote the mean; ns: not significant (Mann–Whitney test). (D) Error bars indicate SEM.

### Time-lapse imaging

Embryos at stage 14–15 of development (11–12 h after egg laying) were dechorionated in 50% bleach for 2 min and rinsed with water. Embryos were aligned on an apple juice–agar pad, glued ventrolateral-side-down onto a coverslip using heptane glue, and covered with a 1:1 mix of halocarbon oil 27 and halocarbon oil 700 (Sigma-Aldrich). A Revolution XD spinning disk confocal (Andor) with a 60 $\times$  oil-immersion lens (NA 1.35; Olympus) was used to image embryos. Images were acquired using an iXon Ultra 897 camera (Andor) and Metamorph (Molecular Devices) as the image acquisition software. Sixteen-bit Z-stacks were acquired at 0.5- to 0.75- $\mu\text{m}$  steps every 3–30 s (7–11 slices per stack). Analysis used maximum intensity projections. The same linear contrast adjustment was applied to all the images in each experiment.

### Injections

Embryos were dechorionated and aligned as above, dehydrated for 15–20 min, and covered in a 1:1 mix of halocarbon oil 27 and halocarbon oil 700. Injections were conducted using a Transferman NK2 micromanipulator (Eppendorf) and a PV820 microinjector (WPI) coupled to our spinning disk confocal. Embryos were injected with 1 mM cytochalasin D (EMD Millipore), 1 mM jasplakinolide (Tocris Biosciences), or 1 mM latrunculin A (Tocris Biosciences) in 50% DMSO; or with 10 mM Y-27632

(Tocris Biosciences) in water; 50% DMSO or water was used as a control.

### zip dsRNA synthesis and validation

DNA templates to create zip dsRNA were generated by genomic PCR, using primers with the T7 promoter sequence (5'-TAATAC-GACTCACTATAGGGAGACCAC-3') added to the 5' ends. The forward primer was

T7-forward-5'-GCACAAAAGTGCACACAGGAA-3', and the reverse primer was:

T7-reverse-5'-TAACCTGCCGTTCTAATGCC-3'.

PCR products were used as templates for in vitro dsRNA synthesis with the T7 MEGAScript kit (Thermo Fisher). RNA was extracted using phenol-chloroform and precipitated in isopropanol. dsRNA was injected in syncytial embryos (0–60 min after egg laying) at concentrations of 1  $\mu\text{g}/\mu\text{l}$ . Water was injected as a control. Embryos were aged at 18 $^{\circ}\text{C}$  for 18 h.

### Laser ablation

A pulsed Micropoint N2 laser (Andor) tuned to 365 nm was used to wound the embryonic epidermis. The laser produced 120- $\mu\text{J}$  pulses with a duration of 2–6 ns. Ten laser pulses were delivered in seven

spots along a 14- $\mu\text{m}$  line to generate a wound. Each embryo was wounded only once. Ten laser pulses were delivered at a single spot to release tension at the wound margin, and samples were imaged immediately before and 1.72 s after spot ablation. In sham-irradiated controls, the laser was completely attenuated using a neutral density filter.

## FRAP

We used a FRAPPA system (Andor) and a 488-nm laser for photobleaching experiments. A 1.7  $\mu\text{m} \times 1.7 \mu\text{m}$  ( $10 \times 10$  pixel) region was photobleached with a dwell time of 500  $\mu\text{s}$ /pixel. Two Z-stacks were acquired 3 s apart prior to photobleaching. Photobleached regions were imaged immediately after photobleaching and then every 3 s for at least 2 min.

Images were registered in SIESTA, an image analysis platform that we developed using MATLAB (MathWorks) (Leung and Fernandez-Gonzalez, 2015). SIESTA was also used to annotate the photobleached region and to measure fluorescence intensities. Custom MATLAB scripts were used to compile the information from multiple images. SIESTA is available for download at [www.quantmorph.ca](http://www.quantmorph.ca).

Fluorescence intensity in the photobleached region at time  $t$ ,  $f(t)$ , was measured as

$$f(t) = 100 * \frac{((I_{\text{ROI}}(t) - I_{\text{bg}}(t)) - (I_{\text{ROI}}(0) - I_{\text{bg}}(0)))}{((I_{\text{ROI}}(\text{before}) - I_{\text{bg}}(\text{before})) - (I_{\text{ROI}}(0) - I_{\text{bg}}(0)))} * \frac{(I_M(\text{before}) - I_{\text{bg}}(\text{before}))}{(I_M(t) - I_{\text{bg}}(t))} \quad (1)$$

where  $t = \text{before}$  is the time immediately before photobleaching,  $t = 0$  is the time immediately after photobleaching,  $I_{\text{ROI}}$  is the mean pixel value within the photobleached region,  $I_{\text{bg}}$  is the background signal, calculated as the mean pixel value within a  $10 \times 10$  pixel region outside the embryo, and  $I_M$  is the mean image intensity. The mobile fraction was the average  $f(t)$  value for the last two time points measured, and  $t_{1/2}$  was the time required to reach half of the mobile fraction.

To extract the rates of actin assembly,  $k_{\text{on}}$ , and disassembly,  $k_{\text{off}}$ , from FRAP experiments, we used a simple two state model (Kobb *et al.*, 2017). Briefly, we assumed that the fluorescent actin reporters can be part of one of two pools, bound to the cortex at the wound edge ( $A_B$ ) or unbound from it ( $A_U$ ). Both  $k_{\text{on}}$  and  $k_{\text{off}}$  represent the rate constants of the transitions between bound and unbound states:



The change in concentration of the bound pool of actin, can be expressed as

$$\frac{dB}{dt} = -k_{\text{off}}B + k_{\text{on}}U \quad (3)$$

where  $B$  and  $U$  are the concentration of  $A_B$  and  $A_U$ , respectively. Assuming equilibrium at short time scales, and that on photobleaching,  $B = 0$ , fluorescence in the photobleached region can be defined as

$$f(t) = \frac{B(t)}{B_{\text{eq}}} \quad (4)$$

where  $B(t)$  is the concentration of  $A_B$  in the photobleached region at time  $t$ . If the total concentration of fluorescent actin in the cell did not change over the course of a FRAP experiment:

$$\frac{df}{dt} = k_{\text{off}} - (k_{\text{off}} + k_{\text{on}})f(t) \quad (5)$$

Solving Eq. 5:

$$f(t) = \frac{k_{\text{off}}}{(k_{\text{off}} + k_{\text{on}})} \left[ 1 - e^{-t(k_{\text{off}} + k_{\text{on}})} \right] \quad (6)$$

$$f(t) = f_{\text{max}} \left[ 1 - e^{-\frac{t}{\tau}} \right] \quad (7)$$

where  $f_{\text{max}}$  is the mobile fraction, and  $\tau$  is a characteristic time scale:

$$f_{\text{max}} = \frac{k_{\text{off}}}{k_{\text{off}} + k_{\text{on}}} \quad (8)$$

$$\tau = \frac{1}{k_{\text{off}} + k_{\text{on}}} \quad (9)$$

We fitted the FRAP data using Eq. 7, and we quantified  $k_{\text{on}}$  and  $k_{\text{off}}$  as

$$k_{\text{on}} = \frac{1 - f_{\text{max}}}{\tau} \quad (10)$$

$$k_{\text{off}} = \frac{f_{\text{max}}}{\tau} \quad (11)$$

## Image analysis

Changes in fluorescence at the wound edge after releasing tension were quantified over time as (Figures 2C and 3C and Supplemental Figure S3C):

$$\% \text{initial fluorescence} = 100 * \frac{I(t)}{I(\text{before})} \quad (12)$$

where  $t$  represents the time after tension release,  $t = \text{before}$  indicates the time before releasing tension, and  $I$  indicates the mean pixel value within a  $3 \times 10$  pixel region of interest on the wound edge, adjacent or far from the site of tension release, or randomly selected in sham-irradiated controls. Mean pixel values were background-subtracted and corrected for photobleaching as above. In addition, we quantified the percentage of change in fluorescence 100 s after tension release (Figures 2C' and 3C' and Supplemental Figure S3C'):

$$\% \text{fluorescence change} = 100 * \frac{[I(100 \text{ s}) - I(\text{before})]}{I(\text{before})} \quad (13)$$

To show that *zip* dsRNA reduces myosin levels (Supplemental Figure S5, A and B), we quantified myosin:GFP fluorescence in epidermal cables. The cables were traced using the LiveWire method, a semiautomated algorithm based on Dijkstra's optimal path search (Dijkstra, 1959) that identifies the brightest pixels between two manually selected points (Fernandez-Gonzalez and Zallen, 2013). Four epidermal cables formed by at least six cell-cell interfaces were

traced per embryo, within a single denticle belt, and the mean intensity of all four cables was averaged to obtain a single intensity value per embryo. The LiveWire algorithm was also used to trace the wound edge and quantify defects in wound closure (Supplemental Figures S5, D and E, S6B, and S9B).

### Statistical analysis

We compared sample means using a nonparametric Mann–Whitney test. To compare more than two groups, we used a Kruskal–Wallis test to reject the null hypothesis and Dunn’s test for pairwise comparison. To compare paired samples (e.g., before and after injection), we used Wilcoxon signed-rank test. For time series, error bars indicate SEM. For box plots, error bars show the SD, the box indicates the SEM, and gray lines denote the mean.

### ACKNOWLEDGMENTS

We are grateful to Jessica Yu for making the *zipper* dsRNA; to Miranda Hunter, Gordana Scepanovic, Jessica Yu, and Teresa Zulueta-Coarasa for comments on the manuscript; to Sérgio Simoes, Michelle Bendeck, Tony Harris, Jon Rocheleau, and Will Ryu for useful discussions; and to Jari Yläne for reagents. Flybase provided important information for this study. Our work was funded by grants to R.F.G. from the Natural Sciences and Engineering Research Council of Canada (418438-13), the Canada Foundation for Innovation (30279), the Ontario Ministry of Economic Development and Innovation (ER14-10-170), the Canada First Research Excellence Fund–University of Toronto Medicine by Design, and the Canadian Institutes of Health Research (156279). K.E.R. is supported by a CIHR Postdoctoral Fellowship. R.F.G. is the Tier II Canada Research Chair in Quantitative Cell Biology and Morphogenesis.

### REFERENCES

Abreu-Blanco MT, Verboon JM, Liu R, Watts JJ, Parkhurst SM (2012). *Drosophila* embryos close epithelial wounds using a combination of cellular protrusions and an actomyosin purse string. *J Cell Sci* 125, 5984–5997.

Antunes M, Pereira T, Cordeiro JV, Almeida L, Jacinto A (2013). Coordinated waves of actomyosin flow and apical cell constriction immediately after wounding. *J Cell Biol* 202, 365–379.

Bertet C, Sulak L, Lecuit T (2004). Myosin-dependent junction remodeling controls planar cell intercalation and axis elongation. *Nature* 429, 667–671.

Brock J, Midwinter K, Lewis J, Martin P (1996). Healing of incisional wounds in the embryonic chick wing bud: characterization of the actin purse-string and demonstration of a requirement for Rho activation. *J Cell Biol* 135, 1097–1107.

Bubb MR, Senderowicz AM, Sausville EA, Duncan KL, Korn ED (1994). Jaspilkinolide, a cytotoxic natural product, induces actin polymerization and competitively inhibits the binding of phalloidin to F-actin. *J Biol Chem* 269, 14869–14871.

Bubb MR, Spector I, Beyer BB, Fosen KM (2000). Effects of jaspilkinolide on the kinetics of actin polymerization. An explanation for certain *in vivo* observations. *J Biol Chem* 275, 5163–5170.

Coue M, Brenner SL, Spector I, Korn ED (1987). Inhibition of actin polymerization by latrunculin-A. *FEBS Lett* 213, 316–318.

Courtemanche N, Lee JY, Pollard TD, Greene EC (2013). Tension modulates actin filament polymerization mediated by formin and profilin. *Proc Natl Acad Sci USA* 110, 9752–9757.

Cramer LP (1999). Role of actin-filament disassembly in lamellipodium protrusion in motile cells revealed using the drug jaspilkinolide. *Curr Biol* 9, 1095–1105.

Davidson LA, Ezin AM, Keller R (2002). Embryonic wound healing by apical contraction and ingression in *Xenopus laevis*. *Cell Motil Cytoskeleton* 53, 163–176.

Dijkstra EW (1959). A note on two problems in connexion with graphs. *Numer Math* 1, 269–271.

Fernandez-Gonzalez R, Simoes Sde M, Roper JC, Eaton S, Zallen JA (2009). Myosin II dynamics are regulated by tension in intercalating cells. *Dev Cell* 17, 736–743.

Fernandez-Gonzalez R, Zallen JA (2013). Wounded cells drive rapid epidermal repair in the early *Drosophila* embryo. *Mol Biol Cell* 24, 3227–3237.

Flanagan MD, Lin S (1980). Cytochalasins block actin filament elongation by binding to high affinity sites associated with F-actin. *J Biol Chem* 255, 835–838.

Gaggioli C, Hooper S, Hidalgo-Carcedo C, Grosse R, Marshall JF, Harrington K, Sahai E (2007). Fibroblast-led collective invasion of carcinoma cells with differing roles for RhoGTPases in leading and following cells. *Nat Cell Biol* 9, 1392–1400.

Hansen SD, Mullins RD (2015). Lamellipodin promotes actin assembly by clustering Ena/VASP proteins and tethering them to actin filaments. *Elife* 4, e06585.

Hayakawa K, Tatsumi H, Sokabe M (2011). Actin filaments function as a tension sensor by tension-dependent binding of cofilin to the filament. *J Cell Biol* 195, 721–727.

Heller E, Kumar KV, Grill SW, Fuchs E (2014). Forces generated by cell intercalation tow epidermal sheets in mammalian tissue morphogenesis. *Dev Cell* 28, 617–632.

Hidalgo-Carcedo C, Hooper S, Chaudhry SI, Williamson P, Harrington K, Leitinger B, Sahai E (2011). Collective cell migration requires suppression of actomyosin at cell-cell contacts mediated by DDR1 and the cell polarity regulators Par3 and Par6. *Nat Cell Biol* 13, 49–58.

Higashida C, Kiuchi T, Akiba Y, Mizuno H, Maruoka M, Narumiya S, Mizuno K, Watanabe N (2013). F- and G-actin homeostasis regulates mechano-sensitive actin nucleation by formins. *Nat Cell Biol* 15, 395–405.

Homem CC, Peifer M (2008). Diaphanous regulates myosin and adherens junctions to control cell contractility and protrusive behavior during morphogenesis. *Development* 135, 1005–1018.

Hu S, Dasbiswas K, Guo Z, Tee YH, Thiagarajan V, Hersen P, Chew TL, Safran SA, Zaidel-Bar R, Bershadsky AD (2017). Long-range self-organization of cytoskeletal myosin II filament stacks. *Nat Cell Biol* 19, 133–141.

Huang J, Zhou W, Dong W, Watson AM, Hong Y (2009). From the cover: directed, efficient, and versatile modifications of the *Drosophila* genome by genomic engineering. *Proc Natl Acad Sci USA* 106, 8284–8289.

Huelsmann S, Rintanen N, Sethi R, Brown NH, Ylanne J (2016). Evidence for the mechanosensor function of filamin in tissue development. *Sci Rep* 6, 32798.

Jegou A, Carlier MF, Romet-Lemonne G (2013). Formin mDia1 senses and generates mechanical forces on actin filaments. *Nat Commun* 4, 1883.

Kiehart DP, Galbraith CG, Edwards KA, Rickoll WL, Montague RA (2000). Multiple forces contribute to cell sheet morphogenesis for dorsal closure in *Drosophila*. *J Cell Biol* 149, 471–490.

Kobb AB, Zulueta-Coarasa T, Fernandez-Gonzalez R (2017). Tension regulates myosin dynamics during *Drosophila* embryonic wound repair. *J Cell Sci* 130, 689–696.

Lee T, Luo L (1999). Mosaic analysis with a repressible cell marker for studies of gene function in neuronal morphogenesis. *Neuron* 22, 451–461.

Leung CY, Fernandez-Gonzalez R (2015). Quantitative image analysis of cell behavior and molecular dynamics during tissue morphogenesis. *Methods Mol Biol* 1189, 99–113.

Martin P, Lewis J (1992). Actin cables and epidermal movement in embryonic wound healing. *Nature* 360, 179–183.

Matsubayashi Y, Coulson-Gilmer C, Millard TH (2015). Endocytosis-dependent coordination of multiple actin regulators is required for wound healing. *J Cell Biol* 210, 677–679.

Mendes Pinto I, Rubinstein B, Kucharavy A, Unruh JR, Li R (2012). Actin depolymerization drives actomyosin ring contraction during budding yeast cytokinesis. *Dev Cell* 22, 1247–1260.

Rauzi M, Lenne PF, Lecuit T (2010). Planar polarized actomyosin contractile flows control epithelial junction remodelling. *Nature* 468, 1110–1114.

Romero S, Le Clainche C, Didry D, Egile C, Pantaloni D, Carlier MF (2004). Formin is a processive motor that requires profilin to accelerate actin assembly and associated ATP hydrolysis. *Cell* 119, 419–429.

Roper K, Mao Y, Brown NH (2005). Contribution of sequence variation in *Drosophila* actins to their incorporation into actin-based structures *in vivo*. *J Cell Sci* 118, 3937–3948.

Royou A, Field C, Sisson J, Sullivan W, Kares R (2004). Reassessing the role and dynamics of nonmuscle myosin II during furrow formation in early *Drosophila* embryos. *Mol Biol Cell* 15, 838–850.

Simone RP, DiNardo S (2010). Actomyosin contractility and Discs large contribute to junctional conversion in guiding cell alignment within the *Drosophila* embryonic epithelium. *Development* 137, 1385–1394.

- Spector I, Shochet NR, Kashman Y, Groweiss A (1983). Latrunculins: novel marine toxins that disrupt microfilament organization in cultured cells. *Science* 219, 493–495.
- Verboon JM, Parkhurst SM (2015). Rho family GTPase functions in *Drosophila* epithelial wound repair. *Small GTPases* 6, 28–35.
- Williams-Masson EM, Malik AN, Hardin J (1997). An actin-mediated two-step mechanism is required for ventral enclosure of the *C. elegans* hypodermis. *Development* 124, 2889–2901.
- Wilson CA, Tsuchida MA, Allen GM, Barnhart EL, Applegate KT, Yam PT, Ji L, Keren K, Danuser G, Theriot JA (2010). Myosin II contributes to cell-scale actin network treadmilling through network disassembly. *Nature* 465, 373–377.
- Wood W, Jacinto A, Grose R, Woolner S, Gale J, Wilson C, Martin P (2002). Wound healing recapitulates morphogenesis in *Drosophila* embryos. *Nat Cell Biol* 4, 907–912.
- Yamashiro S, Tanaka S, McMillen LM, Taniguchi D, Vavylonis D, Watanabe N (2018). Myosin-dependent actin stabilization as revealed by single-molecule imaging of actin turnover. *Mol Biol Cell* 29, 1941–1947.
- Zulueta-Coarasa T, Fernandez-Gonzalez R (2018). Dynamic force patterns promote collective cell movements during embryonic wound repair. *Nat Phys* 14, 750–758.
- Zumdieck A, Kruse K, Bringmann H, Hyman AA, Julicher F (2007). Stress generation and filament turnover during actin ring constriction. *PLoS One* 2, e696.